A portable three-dimensional photoacoustic tomography system for imaging of chronic foot ulcers

Yuehang Wang[1], Ye Zhan[1], Linda M. Harris[2], Sikandar Khan[2], Jun Xia[1]

[1]Department of Biomedical Engineering, [2]Department of Surgery, University at Buffalo, The State University of New York, Buffalo, New York, USA

Correspondence to: Prof. Jun Xia. Department of Biomedical Engineering, University at Buffalo, The State University of New York, Buffalo, New York, USA. Email: junxia@buffalo.edu.

Background: Chronic leg ulcers affect approximately 6.5 million Americans and the disorder is associated with a range of serious complications. Since many chronic ulcers have underlying vascular insufficiency, accurate assessment of tissue perfusion is critical to treatment planning and post-surgical monitoring. However, existing clinical tests fail to meet this need in practice due to their low sensitivity or accuracy.

Methods: In this paper, we introduce a portable photoacoustic tomography (PAT) system for wound assessment. Since hemoglobin serves as the major endogenous contrast at near-infrared wavelengths, PAT provides label-free, three-dimensional (3D) imaging of hemoglobin distribution, which is closely related to blood perfusion. The proposed system consists of a 128-element linear transducer array, a data acquisition (DAQ) system, and a pulsed Nd:YAG laser source, all mounted on a portable cart for easy clinical testing.

Results: We validated our system through both phantom and human imaging studies. The phantom imaging results indicate that the system's spatial resolution ranges from 0.5 mm along the axial direction to 1.3 mm along the elevational direction. The healthy volunteer result shows clear foot vasculature, indicating good perfusion. The preliminary patient imaging results agree very well with the clinical test, demonstrating that PAT has a high potential for assessing the circulation around the wound.

Conclusions: We believe that our technique will be a valuable tool for assessing tissue perfusion and guiding wound treatment in vascular clinics.

Keywords: Photoacoustic tomography (PAT); chronic ulcer; tissue perfusion; vascular imaging

Introduction

Chronic leg ulcers are affecting approximately 6.5 million Americans (1) and the disorder includes venous stasis ulcers, arterial ulcers, pressure ulcers, and diabetic (neuropathic) ulcers. They are associated with significant morbidity, reduced quality of life, and high treatment costs. Annually, over $25 billion is spent in the USA on chronic ulcer treatment, and that burden is steadily growing due to an aging population and rising incidences of both diabetes and obesity (1). Most chronic ulcers have underlying concomitant vascular diseases at both macro- and microvascular levels, which lead to ischemia and delayed or failed healing. In fact, recent studies revealed that critical ischemia-related ulcers are the most severe ulcers and these patients have the longest hospital stays and healing times (2). The 5-year mortality rate is comparable to common types of cancer (3).

One highly effective intervention to chronic ulcers is revascularization surgery, which restores in-line arterial blood flow to ulcers (4). Over the last decade, the angiosome concept has become widely accepted for guiding revascularization. However, in certain patients, particularly diabetics or those with peripheral artery disease (PAD), perfusion to one vessel may be normal, while perfusion to an area of tissue loss may be inadequate (4,5). The ability

800

Wang et al. Photoacoustic imaging of foot ulcers

Table 1 A list of conventional tests for assessing blood perfusion to a wound

Assessment techniques	Limitations
Physical assessment in terms of wound size and color	Subjective, limited information about underlying perfusion and blood flow
Ankle-brachial index (ABI)	Limited accuracy: does not work on non-compressible vessels
Toe-brachial index (TBI)	Limited accuracy: will not work on patients with prior loss of digits
Photoplethysmography (PPG)	Susceptible to local skin conditions: reflux veins affect perfusion measurement
Transcutaneous oxygen pressure (TcPO$_2$)	Lengthy procedure (>45 min): cellulitis or significant foot edema may confound the accuracy

to detect changes after revascularization and determine whether perfusion has been adequately restored would significantly benefit vascular surgeons and specialists caring for patients with tissue loss in their feet (6).

However, current clinical tests for blood perfusion fail to meet this need. As shown in *Table 1*, generalized assessment approaches, such as ankle-brachial pressure index and toe blood pressure readings do not provide information about blood perfusion at a specific region of tissue. They are also subject to errors or limitations due to the inaccurate handhold Doppler device, vessel calcification, and loss of digits (7). Tissue level assessment techniques include photoplethysmography (PPG) and transcutaneous oxygen pressure (TcPO$_2$). However, PPG readings cannot be specific to a single vessel due to the nature of light diffusion and the result is susceptible to local skin conditions and reflex veins (8). TcPO$_2$ requires a lengthy acquisition time (>45 minutes) and the reading is affected by cellulitis or significant foot edema (9). Doppler ultrasound and X-ray CT angiogram have also been used in vascular clinics. However, their primary roles are in the assessment of proximal vessels and these technologies are rarely used in evaluating distal perfusion, due to their low sensitivity to small vessels (Doppler ultrasound) or ionizing radiation (X-ray CT) (9). Recently, various near-infrared imaging techniques have been proposed in wound assessment (10,11). Among them, ICG-based near-infrared fluorescence angiography is probably the most widely studied (9). Upon intravenous injection of ICG, fluorescence images of ICG in tissue can be used to inform tissue perfusion and blood flow. However, the technique has a relatively low rate of clinical adoption, possibly because of two limitations: (I) need for contrast injection, which increases patient discomfort; and (II) light diffusion, which degrades the spatial resolution and imaging depth (2).
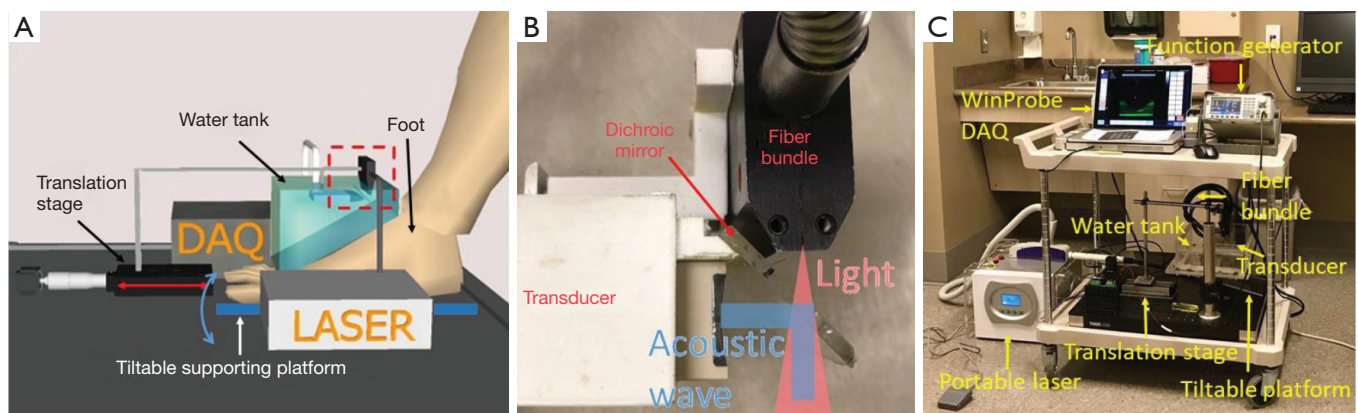
To address these challenges, we proposed a three-dimensional (3D) high-resolution, deep-tissue wound assessment system based on photoacoustic tomography (PAT). PAT is an emerging hybrid imaging modality that provides ultrasonic detection of optical absorption in tissue through the photoacoustic effect. The conversion of optical energy into acoustic energy breaks through the optical diffusion limit, enabling deep-tissue optical absorption to be visualized at a high spatial resolution (12,13). Because blood vessels contain higher concentrations of hemoglobin, PAT can noninvasively map vascular distribution without using any exogenous contrast agents (14,15).

While various PAT systems have been developed for different applications, there are limited reports on a PAT system that is tailored for foot imaging. Here, we introduce our first portable PAT foot imaging system developed based on a custom-made linear transducer array. Two versions of systems were developed. One is built based on bulky laser and ultrasound systems for imaging healthy volunteers in the university lab, while the other is a miniaturized, cart-based system for patient imaging in the vascular clinic. The two systems share the same ultrasound transducer array and fiber bundle for acoustic detection and optical illumination, respectively.

Methods

The proposed system (*Figure 1A*) consists of a custom-made waterproof linear transducer array (IMASONIC, France), a DAQ system, and a Q-switched Nd:YAG laser. The customized waterproof transducer array has 128 elements with 8.6 cm lateral width. The central frequency and focal length of the transducer are 2.25 MHz and 4 cm, respectively. The DAQ unit used for lab testing has 128 channels (Vantage-128, Verasonics Inc.) with 14-bit digital resolution, 54 dB gain, and up to 64 MHz sampling rate. The portable DAQ system (WinProbe, UltraVision Research
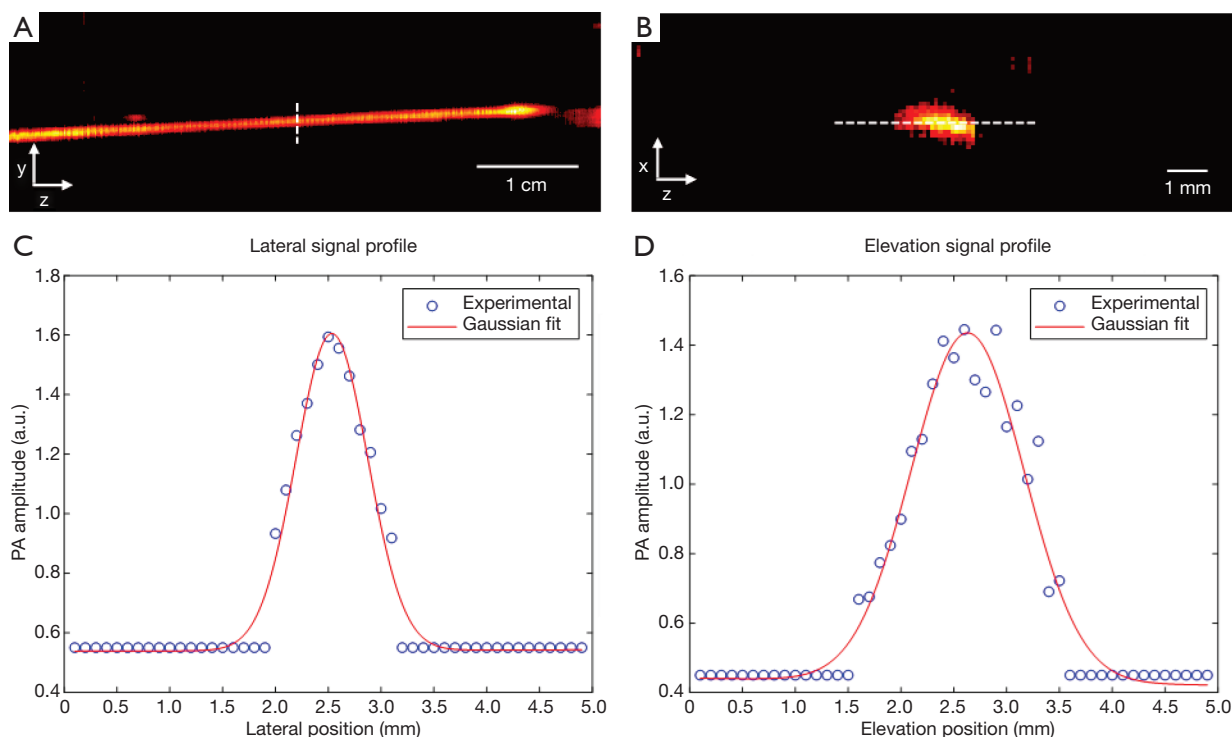
Figure 1 The photoacoustic foot imaging system. (A) Schematic drawing of the imaging system. The red dashed box shows the single-reflector illumination and detection setup and the red double arrow shows the scanning direction. (B) A magnified photograph of the single-reflector illumination and detection setup. The laser beam passes through the reflector, while the photoacoustic signals are reflected by 90 degrees to the transducer array. (C) Photograph of the foot imaging system in a vascular clinic. The system utilizes portable DAQ and laser systems. All components fit in a cart. DAQ, data acquisition.

Platform) (16) used for clinical testing has 64 transmit and receive channels, 14-bit digital resolution, 54 dB gain, and up to 40 MHz sampling rate. Overall, the two systems have comparable acquisition parameters, except that the Winprobe system requires two laser pulses to capture 128 channel data. The lab unit uses a flash-lamp-pumped Continuum™ Nd:YAG laser with 8–10 ns pulse width, 10 Hz pulse repetition frequency (PRF), and up to 800 mJ output power. The portable, consumer-grade Nd:YAG laser has 6–10 ns pulse width, 6 Hz PRF, and up to 200 mJ output power. Both lasers output 1,064 nm wavelength, which can penetrate deep in biological tissue (17). For all human experiments, the light intensity on skin surface was measured to be less than 21 mJ/cm^2, which is well below the ANSI safety limit of 100 mJ/cm^2 for 1,064 nm light (18).

As shown in *Figure 1A*, we used a water tank to couple the foot and the transducer array. The water tank has an opening at the bottom, which was sealed by a 0.05 mm thickness fluorinated ethylene propylene (FEP) plastic film (85905K64, McMaster-Carr). FEP film was chosen here due to its good ductility and negligible acoustic and optical attenuation (as verified experimentally through pulse-echo and optical transmission experiments). The foot was imaged through this film window. As for the light illumination, we adopted the single-reflector illumination method as shown in *Figure 1B* (19). This method effectively achieves co-planar light illumination and acoustic detection. Our double-reflector method could have achieved the same co-planar effect (20), but it was not implemented in this

study because the transducer is already waterproof and can be fully immersed in water. The transducer and the fiber bundle were combined by a 3D printed holder. A dichroic mirror (TECHSPEC® cold mirror, Edmund Optics) was inserted in the middle with a 45-degree angle to the transducer (*Figure 1B*). The dichroic mirror allows for 97% of 1,064 nm light to pass through at 45-degree incident angle. It also reflects the acoustic wave by 90-degrees. For light delivery, we used a fiber bundle with a 1 cm-diameter circular input and 9 cm-length line output (Dolan-Jenner Industries). During the experiment, the transducer array and the fiber bundle were both submerged in water and moved simultaneously along the scanning direction.

As shown in *Figure 1C*, the foot was supported by a tiltable platform, so that the foot surface can be aligned with the imaging window. All system components fit in a portable cart. For different subjects, we determine the scanning time based on the length of the foot and a step size of 0.1 mm per laser pulse. For example, scanning the linear array over 1 cm along the elevational direction takes 10 seconds with 0.1 mm/pulse step size and 10 Hz laser PRF. During all human experiments, ultrasound gel and deionized water were used to minimize air bubbles. To avoid motion artifacts, we asked the subject to stay still during the less than two minutes of imaging time. The water tank and imaging platform also helped to secure the foot in place. We also ensured that the skin-to-transducer distance was around 40 mm, which is the acoustic focal length. At the focal spot, the transducer has the highest elevation resolution.

Figure 2 Characterization of the spatial resolution. (A) Maximum amplitude projection image of a human hair placed along the elevation direction of the transducer array. The z-axis indicates the elevation direction of the array, which is also the scanning direction, and the y-axis indicates the lateral direction of the array. (B) Maximum amplitude projection image of a human hair placed along the lateral direction of the transducer array. The x-axis represents the axial direction of the array. (C) Photoacoustic signal profile along the white-dashed line in (A). (D) Photoacoustic signal profile along the white dashed line in (B). The Gaussian fittings are plotted in red lines.
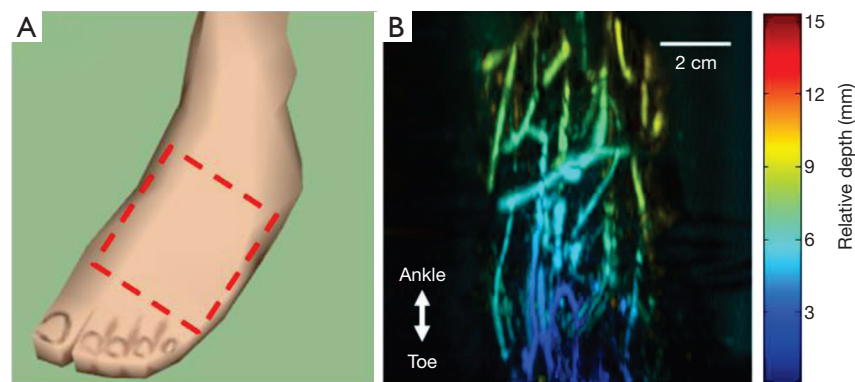
After data acquisition (DAQ), we used the universal back-projection (UBP) algorithm (21) to reconstruct each 2D imaging plane and then stack multiple planes to form a 3D volume image. For better visualization, all reconstructed 3D images were projected along the axial direction of the transducer array to form a maximum amplitude project (MAP) image. Due to the weak output from the portable laser, electronic noises can be seen as horizontal stripes in the MAP image. A stripe removal algorithm was employed to remove the majority of stripe noises in the patient data (22). All human imaging experiments were performed in compliance with the University at Buffalo IRB protocol and all subjects gave informed consent for the imaging study.

Results

The spatial resolution of the system was quantified by imaging a tissue mimic phantom. A black human hair was embedded in an agar gel. As shown in *Figure 2A,B*,

the human hair was placed along either the lateral or the elevation direction of the transducer array for imaging. The distance between the human hair and the transducer was set to 4 cm, which is the acoustic focal length of the array. *Figure 2C,D* show the PA signal profile and Gaussian fitting along the lateral (y) and elevational (z) directions, respectively. The spatial resolution was quantified by the full width at half maximum (FWHM) value, which is 0.7 mm and 1.3 mm along the lateral and elevational directions, respectively. These values agree well with the transducer element pitch and numerical aperture. While the lateral resolution will not very much at different depths, the elevation resolution will degrade quickly as the object moves away from the transducer focus. This issue can be addressed through our 3D reconstruction (23) or slit-PAT technologies (24,25). However, because the purpose of this manuscript is to highlight the first human results, we did not implement those technologies in this study. The axial resolution, while not quantified in *Figure 2*, was around 0.5 mm.

Figure 3 Healthy volunteer results. (A) Schematic drawing of the imaging region (marked by red-dashed box); (B) depth-encoded photoacoustic image of foot instep-bridge region of a healthy volunteer.
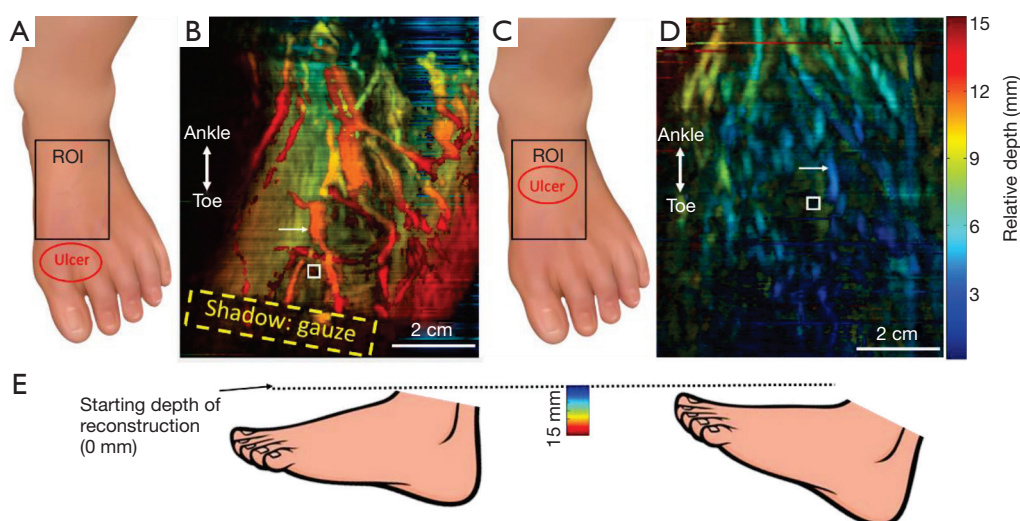
Because all future images were projected along the axial direction, the axial resolution did not play a significant role in this form of image presentation.

To test the *in vivo* imaging capability of our system, we imaged the right foot of a healthy volunteer. During the experiments, the subject was sitting in front of the system and ultrasound gel was applied as the coupling medium between the foot and the plastic film. The region of interest is illustrated in *Figure 3A* and the corresponding photoacoustic image is shown in *Figure 3B*. The photoacoustic image is depth encoded, with different colors representing different depths. Here, the depth represents relative axial distance to the transducer surface (after a certain amount of offset depending on the reconstruction parameters). As expected, clear vasculatures can be seen in the image, indicating good blood circulation. Because the tiltable platform changes the inclination angle of the foot, the relative vessel depth changed from 3 mm at the bottom of the image to 9 mm at the top of the image.

Clinical validation was conducted in the UBMD vascular lab. The inclusion criterion was any person 18 years of age or older with a chronic wound on the foot that is presumed to be due to arterial insufficiency or gangrene. The exclusion criteria were pregnant women and adults unable to consent. As mentioned earlier, the core setup of the clinical system was the same as the one used in healthy volunteer imaging with the exception that the laser and DAQ systems were replaced by portable alternatives. Two exemplary PA images are shown in *Figure 4*. *Figure 4B* displays the PA foot image of a 43-year-old male with diabetes and 1st and 2nd toe amputation. The yellow dashed box shows the amputation covered by the gauze.

Clinical test results from Ankle Brachial Index (ABI) and photoplethysmogram all indicated adequate blood perfusion in the foot. However, the ABI result might not be accurate due to the patient's diabetes. Toe brachial index (TBI) could not be performed at the time due to loss of digits. Moreover, none of these tests could provide direct visualization of the wound environment. In contrast, the PA image provides a clear visualization of vasculature and tissue background, which also indicates good blood perfusion. *Figure 4D* is the PA foot image of a 61-year-old male with PAD. Again, because of the toe loss, TBI could not be conducted. However, both ABI (0.53) and CT angiogram results indicated an ischemic condition and vessel stenosis. The PA image also exhibits weaker vascular and background signals, indicating poor blood perfusion. Similar to the healthy volunteer results, the changes in colors in *Figure 4B,D* are mainly caused by the inclination of the foot. *Figure 4E* shows a schematic drawing of the two feet. The second patient's foot was positioned to have a flatter top surface, and thus most signals are in the blue to green region.

It should be noted that we used maximum amplitude projection to display the image. Based on the orientation and depth of the vessel, the vessel signal at a particular location might be weaker than the surrounding tissue signals. Therefore, some vessels look discontinued in the MAP image. To better quantify tissue perfusion, we calculated the vessel-to-background ratio. Because PAD causes poor blood circulation and chronic wound areas are often associated with leaking vessels, the vessel-to-background ratio will decrease in a poorly perfused tissue. The calculated vessel to background ratios are 23.9 and 15.2 in *Figures 4B,D*, respectively. These values agree with

Figure 4 Patient results. (A) Region of interest (ROI) on the foot of a 43-year-old male patient; (B) depth-encoded foot vascular image of the patient in (A); (C) ROI on the foot of a 61-year-old male patient; (D) depth-encoded foot vascular image of the patient in (C). Black boxes indicate the ROI, red circles indicate the ulcer locations, and white double arrows show the orientation of the foot; (E) schematic drawing of the two feet, indicating different inclination angles, which affect depth encoding.

our observation that a well-perfused tissue has better vessel contrast.

Discussion

We successfully developed a prototype PAT system for imaging foot ulcers. We demonstrated the performance of our system in both healthy volunteers and patients. Our preliminary data clearly demonstrated that PAT has a high potential for assessing circulation around the wound. We also miniaturized the system by using a portable Nd:YAG laser, which operates without an optical table. The entire system was mounted on a cart and could be easily transported between clinics. While imaging of human foot vasculature has been demonstrated by other groups (26), our study represents the first implementation based on a linear transducer array, which is significantly cheaper than curved or spherical transducer arrays. In addition, due to the low system profile, positioning of the patient's foot is very easy and requires little effort from the patient. Most of our studies were conducted within 20 minutes (including the patient preparation time) and had little impact on the clinical workflow.

While encouraging results have been demonstrated, future developments are still needed to further improve user-friendliness and imaging capability. One limitation is that the system can image only the instep-bridge portion

of the foot. However, chronic ulcers can occur in other regions, including the sole and heel; therefore, we will need to develop a more versatile system that can image other regions of the foot. The imaging speed and spatial resolution could also be improved by using a higher speed laser and a higher frequency transducer array, respectively. In addition, once a portable multi-wavelength laser becomes available, we could implement functional imaging of oxy- and deoxy-hemoglobin concentrations (27), which may provide better quantification of tissue perfusion. More patient imaging data are also needed to explore additional photoacoustic features of tissue perfusion. Based on wound research literature, other PA features of tissue perfusion could be absolute photoacoustic amplitude, blood vessel density, oxygen saturation, and vessel curvature (28-31). Quantifying these parameters will require multi-wavelength imaging, precise calibration of optical fluence, and a higher frequency transducer array. Nevertheless, with continuing development in PAT technologies, we expect that PAT systems will be widely used in vascular clinics for assessment of tissue perfusion. The technique will facilitate post-surgical decision-making and provide longitudinal monitoring of functional wound information until complete healing.

Acknowledgments

for Advancing Translational Sciences of the National Institutes of Health under award number UL1TR001412 to the University at Buffalo.

Footnote

Conflicts of Interest: The authors have no conflicts of interest to declare.

Ethical Statement: All human imaging experiments were performed in compliance with the University at Buffalo IRB protocol and all subjects were given informed consent for the imaging study.

References

1. Sen CK, Gordillo GM, Roy S, Kirsner R, Lambert L, Hunt TK, Gottrup F, Gurtner GC, Longaker MT. Human Skin Wounds: A Major and Snowballing Threat to Public Health and the Economy. Wound Repair Regen 2009;17:763-71.
2. Mennes O, Slart R, Steenbergen W. Novel Optical Techniques for Imaging Microcirculation in the Diabetic Foot. Curr Pharm Des 2018;24:1304-16.
3. Escandon J, Vivas AC, Tang J, Rowland KJ, Kirsner RS. High mortality in patients with chronic wounds. Wound Repair Regen 2011;19:526-8.
4. Attinger CE, Evans KK, Bulan E, Blume P, Cooper P. Angiosomes of the foot and ankle and clinical implications for limb salvage: reconstruction, incisions, and revascularization. Plast Reconstr Surg 2006;117:261S-93S.
5. Sumpio BE, Forsythe RO, Ziegler KR, van Baal JG, Lepantalo MJ, Hinchliffe RJ. Clinical implications of the angiosome model in peripheral vascular disease. J Vasc Surg 2013;58:814-26.
6. Braun JD, Trinidad-Hernandez M, Perry D, Armstrong DG, Mills JL. Early quantitative evaluation of indocyanine green angiography in patients with critical limb ischemia. J Vasc Surg 2013;57:1213-8.
7. Frykberg RG, Banks J. Challenges in the Treatment of Chronic Wounds. Adv Wound Care (New Rochelle) 2015;4:560-82.
8. Allen J. Photoplethysmography and its application in clinical physiological measurement. Physiol Meas 2007;28:R1.
9. Venermo M, Settembre N, Albäck A, Vikatmaa P, Aho P-S, Lepäntalo M, Inoue Y, Terasaki H. Pilot assessment of the repeatability of indocyanine green fluorescence imaging

and correlation with traditional foot perfusion assessments. Eur J Vasc Endovasc Surg 2016;52:527-33.
10. Sowa MG, Kuo WC, Ko AC, Armstrong DG. Review of near-infrared methods for wound assessment. J Biomed Opt 2016;21:091304.
11. Zhang S, Gnyawali S, Huang J, Ren W, Gordillo G, Sen CK, Xu R. Multimodal imaging of cutaneous wound tissue. J Biomed Opt 2015;20:016016.
12. Wang LV, Yao J. A practical guide to photoacoustic tomography in the life sciences. Nat Methods 2016;13:627.
13. Xia J, Yao J, Wang LHV. Photoacoustic Tomography: Principles and Advances. Electromagn Waves (Camb) 2014;147:1-22.
14. Wang Y, Li Z, Vu T, Nyayapathi N, Oh KW, Xu W, Xia J. A Robust and Secure Palm Vessel Biometric Sensing System based on Photoacoustics. IEEE Sensors J 2018;18:5993-6000.
15. Irisawa K, Hirota K, Hashimoto A, Murakoshi D, Ishii H, Tada T, Wada T, Hayakawa T, Azuma R, Otani N, editors. Photoacoustic imaging system for peripheral small-vessel imaging based on clinical ultrasound technology. International Society for Optics and Photonics: SPIE BiOS, 2016.
16. Lim HT, Matham MV. Hybrid-modality ocular imaging using a clinical ultrasound system and nanosecond pulsed laser. J Med Imaging (Bellingham) 2015;2:036003.
17. Zhou Y, Wang D, Zhang Y, Chitgupi U, Geng J, Wang Y, Zhang Y, Cook TR, Xia J, Lovell JF. A Phosphorus Phthalocyanine Formulation with Intense Absorbance at 1000 nm for Deep Optical Imaging. Theranostics 2016;6:688.
18. Institute ANS. American national standard for safe use of lasers. Laser Institute of America, 2007.
19. Montilla LG, Olafsson R, Bauer DR, Witte RS. Real-time photoacoustic and ultrasound imaging: a simple solution for clinical ultrasound systems with linear arrays. Phys Med Biol 2013;58:N1-12.
20. Wang Y, Lim RSA, Zhang H, Nyayapathi N, Oh KW, Xia J. Optimizing the light delivery of linear-array-based photoacoustic systems by double acoustic reflectors. Sci Rep 2018;8:13004.
21. Xu M, Wang LV. Universal back-projection algorithm for photoacoustic computed tomography. Biomedical Optics 2005 2005:251-4.
22. Münch B, Trtik P, Marone F, Stampanoni M. Stripe and ring artifact removal with combined wavelet—Fourier filtering. Opt Express 2009;17:8567-91.
23. Wang D, Wang Y, Zhou Y, Lovell JF, Xia J. Coherent-

806

Wang et al. Photoacoustic imaging of foot ulcers

weighted three-dimensional image reconstruction in linear-array-based photoacoustic tomography. Biomed Opt Express 2016;7:1957-65.

24. Wang Y, Wang D, Zhang Y, Geng J, Lovell JF, Xia J. Slit-enabled linear-array photoacoustic tomography with near isotropic spatial resolution in three dimensions. Opt Lett 2016;41:127-30.

25. Wang Y, Wang D, Hubbell R, Xia J. Second generation slit-based photoacoustic tomography system for vascular imaging in human. J Biophotonics 2017;10:799-804.

26. Nagae K, Asao Y, Sudo Y, Murayama N, Tanaka Y, Ohira K, Ishida Y, Otsuka A, Matsumoto Y, Saito S. Real-time 3D Photoacoustic Visualization System with a Wide Field of View for Imaging Human Limbs. F1000Res 2018;7:1813.

27. Yao J, Wang L, Yang JM, Maslov KI, Wong TTW, Li L, Huang CH, Zou J, Wang LV. High-speed label-free

28. Kang Y, Choi M, Lee J, Koh GY, Kwon K, Choi C. Quantitative analysis of peripheral tissue perfusion using spatiotemporal molecular dynamics. PLoS One 2009;4:e4275.

29. Matsumoto Y, Asao Y, Yoshikawa A, Sekiguchi H, Takada M, Furu M, Saito S, Kataoka M, Abe H, Yagi T. Label-free photoacoustic imaging of human palmar vessels: a structural morphological analysis. Sci Rep 2018;8:786.

30. Sun C, Munn LL. Lattice-Boltzmann simulation of blood flow in digitized vessel networks. Comput Math Appl 2008;55:1594-600.

31. Li WW, Carter MJ, Mashiach E, Guthrie SD. Vascular assessment of wound healing: a clinical review. Int Wound J 2017;14:460-9.

functional photoacoustic microscopy of mouse brain in action. Nat Methods 2015;12:407-10.